Title	Numerical Simulation of Ionic Mass-Transfer Rates with Natural Convection in CuSO4-H2SO4 Solution
Author(s)	Kawai, S.; Fukunaka, Y.; Kida, S.
Citation	JOURNAL OF THE ELECTROCHEMICAL SOCIETY (2009), 156(9): F99-F108
Issue Date	2009
URL	http://hdl.handle.net/2433/109932
Right	© 2009 The Electrochemical Society
Type	Journal Article
Textversion	publisher

Journal of The Electrochemical Society, **156** (9) F99-F108 (2009)
0013-4651/2009/156(9)/F99/10/$25.00 © The Electrochemical Society

Numerical Simulation of Ionic Mass-Transfer Rates with Natural Convection in $CuSO_4$–H_2SO_4 Solution

I. Numerical Study on the Developments of Secondary Flow and Electrolyte Stratification Phenomena

S. Kawai,[a] Y. Fukunaka,[b,*,z] and S. Kida[a]

[a]*Department of Mechanical Engineering and Science, Kyoto University, Kyoto 606-8501, Japan*
[b]*Nano Technology Research Center, Waseda University, Tokyo 162-0041, Japan*

The ionic mass-transfer rates accompanying natural convective electrolyte flow in a $CuSO_4$ aqueous electrolyte solution acidified with an excess amount of H_2SO_4 are numerically analyzed. The effects of a supporting electrolyte and an interaction behavior between both cathodic upward and anodic downward natural convections are examined. Both anodic and cathodic current density distributions along the vertical height are also calculated. A mathematical model is extended by incorporating an additional boundary condition at the limiting current. A measure of ionic migration effect ε, a ratio of limiting current to limiting diffusion current, involving the transference number of a discharging metallic ion is introduced for this purpose. The present calculation predicts the oscillation behaviors in transient variations in both electrode surface concentration and maximal natural convective velocity, which are deeply related to the periodic fluctuating electrolyte flow patterns distorted by secondary flow. The addition of H_2SO_4 maintains an ε value around 1 and prevents the further development to the transition or turbulent natural convection.
 [DOI: 10.1149/1.3158827]

Manuscript submitted September 23, 2008; revised manuscript received May 27, 2009. Published July 9, 2009.

Natural convective electrolyte flow plays an essential role in several electrochemical reactors. Copper refining electrolysis is the most important industrial process in producing high purity copper in a large scale, where 1 m high vertical-plane electrode surfaces are placed face to face, separated by a 3–5 cm thick electrolyte layer. A supporting electrolyte of H_2SO_4 is frequently added to increase the conductivity of the bath and to improve the polarization parameter for electrodeposition. During the electrolysis, four concentration boundary layers (CBLs) for Cu^{2+}, H^+, HSO_4^-, and SO_4^{2-} ions are formed near both electrode surfaces. They are not completely independent of each other because the electroneutrality condition and acid–base equilibrium must be satisfied.

The investigation applying the physicochemical hydrodynamics to verify the importance of natural convective electrolyte flow was reported by Wagner.[1] Since then, numerous papers have been published on the ionic mass-transfer rate accompanying natural convection developed along the vertical-plane electrodes.[2-11] They are mostly based on the boundary-layer theory in semi-infinite media. The interaction behavior between cathodic upward and anodic downward natural convections has not been frequently discussed.

In the previous study, the effect of the interaction behavior between anodic downward and cathodic upward natural convections developing during the galvanostatic electrolysis in a tiny electrolytic cell was examined both numerically and experimentally.[12] The transient variations in the ionic mass-transfer phenomena associated with modulating an electrolytic current were also investigated.[13] The applied current densities employed in these studies were far below the limiting one, and copper electrolysis was carried out only in a binary $CuSO_4$ aqueous electrolyte solution. Besides, the uniformity of both anodic and cathodic current-density distributions along the vertical height was assumed.

Many theoretical and numerical studies on the current-density distribution were reported as well as on the ionic mass-transfer phenomena in various electrochemical systems such as the rotating-disk electrode system,[14-18] and parallel or tubular electrode systems.[19-24] However, only a few studies have been carried out on the current-density distribution in the vertical-plane electrode system.[6,8,25,26] It is thus indispensable to investigate the transient ionic mass-transfer phenomena accompanying natural convections developing along both electrode surfaces during the galvanostatic copper electrolysis at an appreciable fraction of the limiting current density.

* Electrochemical Society Active Member.
z E-mail: fukunaka@energy.kyoto-u.ac.jp

The goal of this research is to predict the transient behavior of the ionic mass-transfer rates and the current-density distributions along vertical-plane electrodes resulting from an interaction between upward and downward natural convections. The predictions of both limiting current density and criterion of uniform current-density distribution are also necessary to improve the industrial productivity of the electrolytic process with a higher current density. Moreover, it is well known that the ionic mass-transfer rate considerably couples with the microstructural or morphological variations in the electrodeposited film at a relatively high cathodic overpotential. The prediction of the electrode surface overpotential without mass-transfer contribution may provide a key to control the physical and electrical properties of electrodeposited copper films. Numerical simulations may give various insights into the coupling phenomena between the microstructural or morphological variations and the ionic mass-transfer rate.[27]

A mathematical model is developed for a $CuSO_4$ aqueous electrolyte solution acidified with an excess amount of H_2SO_4 under the presumptions of electroneutrality, acid–base equilibrium, and constant physical properties. The effects of supporting electrolyte and interaction between both natural convections are now focused. Calculated results are compared to the optical measurements.[10,11] The present paper addresses only the numerical study part. The comparisons between present numerical calculations and optical measurements are separately carried out in Part II.

Experimental

The experimental setup employed in the present study was the same as previous studies.[10,11] Figure 1 shows a schematic diagram of an electrolytic cell. Both the anode and cathode were vertically installed face to face in a cell, separated by a 4.8 cm thick electrolyte layer. The electrolyte solution was poured into the cell until its surface was positioned at a height of 16 cm from the bottom. Two electrolyte compositions, 0.05 M $CuSO_4$ and 0.05 M $CuSO_4$–1.85 M H_2SO_4 aqueous electrolyte solutions, were employed. A constant electrolytic current was applied to the cathode. The preliminary experiments showed that the cathodic limiting current densities of both electrolyte solutions were about $i = 4.6$ and 2.0 mA/cm^2, respectively.[10] The electrolytic conditions employed in this study are summarized in Table I.

Mathematical Model

A mathematical model and numerical calculation procedure for a binary $CuSO_4$ aqueous electrolyte solution have been reported previously.[12,13] The present study describes a mathematical model

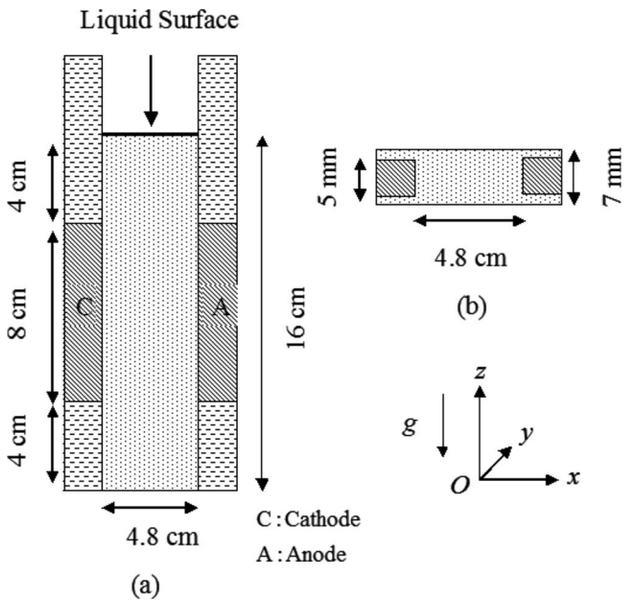

Figure 1. Schematic diagram of the electrolytic cell. (a) Side view and (b) top view.

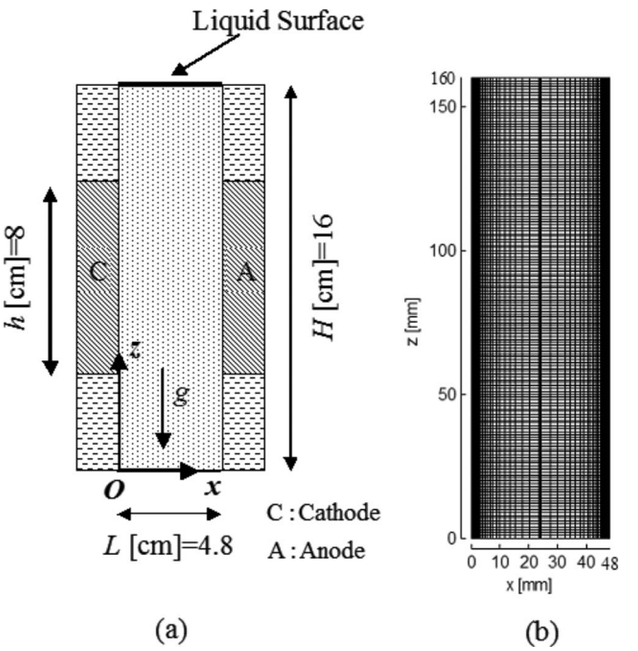

Figure 2. (a) Schematic diagram of the 2D electrolytic cell and (b) unevenly divided grid used in numerical calculation.

for a $CuSO_4$ aqueous electrolyte solution acidified with an excess amount of H_2SO_4. A two-dimensional (2D) mathematical model is numerically analyzed based on the marker-and-cell (MAC) method, using the finite difference method and deterministic relaxation techniques. Figure 2a shows a schematic diagram of the 2D electrolytic cell filled with an aqueous electrolyte. We use a grid of 120 $\times$ 160 cells with an irregular interval mesh, as demonstrated in Fig. 2b, where the minimal mesh size in the vicinity of both electrode surfaces is set to 1 μm which is far larger than the double-layer thickness. The common ratio of less than 1.15 is employed to define the uneven mesh size represented by a geometrical progression.

In a $CuSO_4$–H_2SO_4 electrolyte, both $CuSO_4$ and H_2SO_4 dissociate into four ion species, Cu^{2+}, H^+, HSO_4^-, and SO_4^{2-}, whose concentrations are denoted as C_1, C_2, C_3, and C_4, respectively. When the concentrations of $CuSO_4$ and H_2SO_4 are given as m_A and m_B, respectively, and the degree of dissociation of the HSO_4^- ion is also assigned as a, the following expressions are derived according to the acid–base equilibrium

$$C_1 = m_A \quad C_2 = (1 + a)m_B \quad C_3 = (1 - a)m_B \quad C_4 = m_A + am_B \tag{1}$$

These ion concentrations satisfy the principle of electroneutrality

$$\sum_{k=1}^{4} z_k C_k = 0 \tag{2}$$

Here, z_k is the valency of an ion species k.

Table I. Experimental conditions.

Composition of electrolyte	0.05 M $CuSO_4$
Average current density i_{ave} (mA/cm^2)	0.236, 0.473, 0.946, 1.42, 1 96, 3.65, 4.6
Composition of electrolyte	0.05 M $CuSO_4$–1.85 M H_2SO_4
Average current density i_{ave} (mA/cm^2)	0.236, 0.473, 0.946, 1.42, 1.96
Electrode spacing L (cm)	4.8
Temperature T (K)	293

The mathematical model includes the unsteady convection–diffusion equations for electroneutral compounds $CuSO_4$ and H_2SO_4, the Poisson equation for the electric potential, and the Navier–Stokes and continuity equations for the incompressible viscous fluid. The following equations are derived from the mass and momentum conservation laws under the assumptions of the electroneutrality and constant physical properties

$$\frac{\partial m_A}{\partial t} + (\mathbf{v} \cdot \nabla)m_A = D_A \nabla^2 m_A \tag{3}$$

$$\frac{\partial m_B}{\partial t} + (\mathbf{v} \cdot \nabla)m_B = D_B \nabla^2 m_B \tag{4}$$

$$\nabla^2 \phi = 0 \tag{5}$$

$$\frac{\partial \mathbf{v}}{\partial t} + (\mathbf{v} \cdot \nabla)\mathbf{v} = -\frac{1}{\rho_0} \nabla P + \nu \nabla^2 \mathbf{v} + \frac{\mathbf{f}}{\rho_0} \tag{6}$$

$$\nabla \cdot \mathbf{v} = 0 \tag{7}$$

Here, D_k expresses the diffusion coefficient, ϕ the electric potential, $\mathbf{v}$ the fluid velocity vector, P the pressure, ν the kinematic viscosity, ρ_0 the reference fluid density, and t the time coordinate. $\mathbf{f}$ is an external force vector acting over the fluid. The buoyancy induced by fluid density difference is considered in the present study

$$\mathbf{f} = (\rho - \rho_0)\mathbf{g} \tag{8}$$

Here, ρ is the fluid density and $\mathbf{g}$ is the gravitational acceleration vector. According to the electroneutrality and Boussinesq approximation, the density difference with respect to the concentration of each ion can be described as follows

$$\Delta\rho = \rho - \rho_0 = \rho_0 \left[\left(\frac{1}{\rho_0} \frac{\partial \rho}{\partial m_A} \right) \Delta m_A + \left(\frac{1}{\rho_0} \frac{\partial \rho}{\partial m_B} \right) \Delta m_B \right]$$

$$\therefore \frac{\Delta\rho}{\rho_0} = (\alpha_A \Delta m_A + \alpha_B \Delta m_B) \quad [9]$$

Here, α_A and α_B express the densification coefficients of $CuSO_4$ and H_2SO_4, respectively.

The boundary condition on the electrode surface must be formulated. The no-slip boundary condition is applied. The net mass flux of each ion species k on the electrode surface j_k can be expressed according to the Nernst–Planck equation for the concentration of each ion governed by diffusion and ionic migration as follows

$$j_k = -D_k \frac{\partial C_k}{\partial x} - \mu_k C_k \frac{\partial \phi}{\partial x} \quad [10]$$

Here, μ_k is the mobility of each ion. At the initial condition, the concentration of each ion is set equal to the bulk electrolyte concentration, and the concentration gradient of each ion is absent. Then, the current density i can be written as follows

$$i = F\sum_{k=1}^{4} z_k j_k = -F\left(\sum_{k=1}^{4} \mu_k z_k C_{k,0}\right) \cdot \left(\frac{\partial \phi}{\partial x}\right) = -\sigma\left(\frac{\partial \phi}{\partial x}\right) \quad [11]$$

Here, σ is the electric conductivity of an electrolyte and F is the Faraday constant. The present study assumes that only the Cu^{2+} ion reacts at the electrode/electrolyte interface, and no other electrochemical reaction such as the gas evolution takes place. The boundary condition for each ion on the electrode surface can then be expressed as follows

$$-D_1 \frac{\partial C_1}{\partial x} = \frac{i}{z_1 F}(1.0 - {}^*t_1) \quad [12]$$

$$-D_k \frac{\partial C_k}{\partial x} = \frac{i}{z_k F}(-{}^*t_k) \quad (k = 2,3,4) \quad [13]$$

$${}^*t_k = \frac{\mu_k z_k C_{k,0}}{\sum_{l=1}^{4} \mu_l z_l C_{l,0}} \quad [14]$$

Here, ${}^*t_k$ is the transference number of an ion species k, which represents the ionic migration effect at the electrode surface.

During the electrolysis, the CBLs develop due to the electrochemical deposition and dissolution of copper at the electrode/electrolyte interface. The boundary condition for each ion can be written as follows

$$j_1 = -D_1 \frac{\partial C_1}{\partial x} - \mu_1 C_1 \frac{\partial \phi}{\partial x} = \frac{i}{z_1 F} \quad [15]$$

$$j_k = -D_k \frac{\partial C_k}{\partial x} - \mu_k C_k \frac{\partial \phi}{\partial x} = 0 \quad (k = 2,3,4) \quad [16]$$

According to the electroneutrality, the following equation can be obtained

$$\sum_{k=1}^{4} z_k \frac{\partial C_k}{\partial x} = 0$$

$$\therefore \left(\frac{\partial \phi}{\partial x}\right) = -\frac{i}{z_1 F} \cdot \frac{z_1/D_1}{\sum_{k=1}^{4} \mu_k z_k C_k/D_k} \quad [17]$$

Then, Eq. 15 and 16 can be rewritten as follows

$$\left(\frac{\partial C_1}{\partial x}\right) = -\frac{i}{z_1 F D_1}\left[1.0 - \frac{\mu_1 z_1 C_1/D_1}{\sum_{k=1}^{4} \mu_k z_k C_k/D_k}\right] \quad [18]$$

$$\left(\frac{\partial C_k}{\partial x}\right) = \frac{i}{z_k F D_1}\left[\frac{\mu_k z_k C_k/D_k}{\sum_{l=1}^{4} \mu_l z_l C_l/D_l}\right] \quad (k = 2,3,4) \quad [19]$$

Substitution of Eq. 1 into Eq. 18 and 19 yields the following relation

$$\left(\frac{\partial C_2}{\partial x}\right) = -\xi\left(\frac{\partial C_1}{\partial x}\right) \quad [20]$$

where

$$\xi = \frac{(1.0 + a)m_B}{2m_A + (1.0 + 2a)m_B} \approx \frac{1.0 + a}{1.0 + 2a} \quad (\text{for } m_A \ll m_B) \quad [21]$$

In the above derivation, the following Einstein relation is also applied

$$D_i = \mu_i \frac{RT}{z_i F} \quad [22]$$

Here, R is the universal gas constant and T is the temperature. Similarly, the following relations are derived

$$\left(\frac{\partial C_3}{\partial x}\right) = \eta\left(\frac{\partial C_1}{\partial x}\right) \quad [23]$$

$$\left(\frac{\partial C_4}{\partial x}\right) = \zeta\left(\frac{\partial C_1}{\partial x}\right) \quad [24]$$

where

$$\eta = \frac{(1.0 - a)m_B}{2m_A + (1.0 + 2a)m_B} \approx \frac{1.0 - a}{1.0 + 2a} \quad (\text{for } m_A \ll m_B) \quad [25]$$

$$\zeta = \frac{2(m_A + am_B)}{2m_A + (1.0 + 2a)m_B} \approx \frac{2a}{1.0 + 2a} \quad (\text{for } m_A \ll m_B) \quad [26]$$

In a 0.05 M $CuSO_4$–1.85 M H_2SO_4 electrolyte solution, the degree of dissociation of the HSO_4^- ion is 0.31.[9,10] ξ, η, and ζ can then be approximated as 0.81, 0.43, and 0.38, respectively. These values of ξ, η, and ζ can be estimated as 0.7825, 0.412, and 0.217, respectively, under the consideration of $m_A/m_B = 0.027$ at the initial bulk electrolyte condition. Therefore, this approximation is less accurate particularly in ζ. Both the accuracy improvement and associating consideration of the dependences of physical properties on the electrolyte composition and concentration are left for future work.

The following boundary conditions for the concentration of $CuSO_4$ and the electric potential are derived under the presumption of constant physical properties

$$-D_A \frac{\partial m_A}{\partial x} = \frac{(1.0 - {}^*t_1)}{z_1 F} i \quad [27]$$

$$-\frac{z_1 F}{RT[\zeta - \xi + \eta]} D_A\left(m_A \frac{\partial \phi}{\partial x}\right) = \frac{(1.0 - {}^*t_1)}{z_1 F} i$$

$$D_A = \frac{-\mu_4 D_1 + \mu_1[\zeta - \xi + \eta]D_4}{-\mu_4 + \mu_1[\zeta - \xi + \eta]}$$

$${}^*t_1 = \frac{\mu_1[\zeta - \xi + \eta]}{-\mu_4 + \mu_1[\zeta - \xi + \eta]} \quad [28]$$

Here, D_A and ${}^*t_1$ can be considered as the diffusion coefficient of $CuSO_4$ and the transference number of the Cu^{2+} ion in a $CuSO_4$ aqueous electrolyte solution containing an excess amount of H_2SO_4. Clearly the diffusion coefficient of $CuSO_4$ can be expressed by combining ion diffusivities D_i with mobilities μ_i. Therefore, D_A can be considered as the "binary electrolyte diffusion coefficient,"[28-30] extended to the case of a binary electrolyte solution containing an excess amount of the supporting electrolyte. Then, the following relation between concentration gradients of $CuSO_4$ and H_2SO_4 toward the electrode surface can be obtained

$$\left(\frac{\partial m_B}{\partial x}\right) = -\frac{\xi}{1.0 + a}\left(\frac{\partial m_A}{\partial x}\right) = \frac{(1.0 - {}^*t_1)\xi}{(1.0 + a)D_A}\frac{i}{z_1 F} \quad [29]$$

Assuming that the boundary condition for H_2SO_4 can be similarly expressed as Eq. 13, the diffusion coefficient of H_2SO_4 in a

$CuSO_4$–H_2SO_4 electrolyte solution can be estimated as follows

$$-D_B\frac{\partial m_B}{\partial x} = \frac{(-{}^*t_2)i}{(1.0+a)z_2F} \quad [30]$$

$$D_B = D_A\frac{1}{\xi}\frac{z_1}{z_2}\frac{{}^*t_2}{1.0-{}^*t_1} \quad [31]$$

The current-density distribution along the vertical-plane electrode is also calculated. The electric-potential gradient toward the effective electrode surface is corrected from the constraint that the integration of local current density over the whole effective electrode surface area must be equal to the applied average current density i_{ave}

$$i_C(z) = -\frac{z_1^2F^2}{(1.0-{}^*t_1)RT[\zeta-\xi+\eta]}D_A\left[m_A(z)\frac{\partial\phi(z)}{\partial x}\right]$$

$$i_A(z) = -\frac{z_1^2F^2}{(1.0-{}^*t_1)RT[\zeta-\xi+\eta]}D_A\left[m_A(z)\frac{\partial\phi(z)}{\partial x}\right] \quad [32]$$

$$\int i_C dA = \int i_A dA = i_{ave}\cdot A \quad [33]$$

Here, A denotes the total effective electrode surface area.

The cathode surface Cu^{2+}-ion concentration inevitably starts to considerably vary along the electrode height. When a high level constant electrolytic current is imposed, the limiting current condition may be partially established where the cathode surface concentration of the Cu^{2+} ion approaches zero. Because the present study assumes that only the electrochemical deposition and dissolution of copper are taken into account at the electrode/electrolyte interface and no other reaction such as gas evolution is considered, the electric-potential gradient toward the cathode surface approaches infinity near the limiting current density, as easily imagined in Eq. 32 at $m_A(z)\to 0$. Then, the above-mentioned calculation procedure becomes inevitably unstable. In such a situation, the cathodic current density is expressed exclusively with the concentration gradient

$$\text{If } m_A(z) < 0.05\times m_{A,0}$$

$$i_C(z) = -\frac{z_1F}{(1.0-{}^*t_1)}D_A\left[\frac{\partial m_A(z)}{\partial x}\right]$$

$$\text{If } m_A(z) \geq 0.05\times m_{A,0}$$

$$i_C(z) = -\frac{z_1^2F^2}{(1.0-{}^*t_1)RT[\zeta-\xi+\eta]}D_A\left[m_A(z)\frac{\partial\phi(z)}{\partial x}\right] \quad [34]$$

$$\int i_C dA = i_{ave}\cdot A \quad [35]$$

The present study conventionally assumes that the limiting current condition is substantially established when the concentration of the Cu^{2+} ion at the cathode surface drops below 5% of bulk concentration which corresponds to 2.5×10^{-3} M.

When the whole effective cathode surface reaches the limiting current condition, a correction factor ε involving the transference number of the Cu^{2+} ion is introduced. It is not based on the quantitative technical arguments, but a technique to overcome the computational difficulty. Because the Cu^{2+} ion is no longer a dominant ionic species near the cathode surface at the limiting current condition, the conventional transference number treatment may no longer be accepted. The ratio $\varepsilon = I_L/I_D$ of the limiting current to the limiting diffusion current is a convenient measure of the ionic migration effect, which depends on the electrolyte composition[29]

$$i_{D,C}(z) = -z_1FD_A\left[\frac{\partial m_A(z)}{\partial x}\right] \quad [36]$$

$$I_D = \int i_{D,C}dA$$

$$I_L = i_{ave}\cdot A$$

$$i_C(z) = \varepsilon\cdot i_{D,C}(z) = \frac{I_L}{I_D}i_{D,C}(z) \quad [37]$$

The boundary conditions at both insulated wall and electrolyte free surfaces are described. Because no electrochemical reaction occurs at these interfaces, the boundary conditions on both insulated wall and electrolyte free surfaces are given as follows

$$\frac{\partial m_A}{\partial n} = \frac{\partial m_B}{\partial n} = \frac{\partial\phi}{\partial n} = 0 \quad [38]$$

Here n indicates the normal direction to these boundaries.

The boundary conditions for fluid velocity and pressure fields on both effective electrode and insulated wall surfaces are written as follows, according to the no-slip boundary condition

$$u(x_S,z_S) = 0 \quad w(x_S,z_S) = 0 \quad [39]$$

$$\left[\frac{\partial P(z_S)}{\partial x}\right]_{x=x_S} = \rho_0\nu\nabla^2u(x_S,z_S) \quad [40]$$

The boundary conditions on the bottom wall surfaces are also expressed as follows

$$u(x_{WS},z_{WS}) = 0 \quad w(x_{WS},z_{WS}) = 0 \quad [41]$$

$$\left[\frac{\partial P(x_{WS})}{\partial z}\right]_{z=z_{WS}} = \rho_0\nu\nabla^2w(x_{WS},z_{WS}) - \rho_0g(\alpha_A\Delta m_A + \alpha_B\Delta m_B) \quad [42]$$

The boundary conditions on an electrolyte free surface are written as follows

$$\left[\frac{\partial u(x_{LS})}{\partial z}\right]_{z=z_{LS}} = 0 \quad w(x_{LS},z_{LS}) = 0 \quad [43]$$

$$\left[\frac{\partial P(x_{LS})}{\partial z}\right]_{z=z_{LS}} = \rho_0\nu\nabla^2w(x_{LS},z_{LS}) - \rho_0g(\alpha_A\Delta m_A + \alpha_B\Delta m_B) \quad [44]$$

An electrolyte solution is initially homogeneous and at rest

$$m_A = m_{A,0} = 0.05 \quad m_B = m_{B,0} = 1.85 \quad \mathbf{v} = (u,w) = (0,0) \quad (\text{for } t = 0) \quad [45]$$

The initial condition for the electric potential can be determined according to Eq. 11

$$\frac{\partial\phi(z)}{\partial x} = -\frac{i_{ave}}{\sigma} \quad \text{(effective electrode surface region)}$$

$$\frac{\partial\phi(z)}{\partial x} = 0 \quad \text{(insulated electrode surface region)} \quad [46]$$

In the discretization of governing equations, the second-order central difference scheme is applied for space discretization except for the convective terms, for which the third-order upwind (Kawamura) difference scheme is adopted. Besides, the first-order backward difference scheme is applied for time discretization. The brief flow chart of numerical calculation at each time step is given as follows.

1. The electric-potential field is numerically calculated by solving Eq. 5 with boundary conditions, where the iterative method is employed.

Table II. Physical constants.

Composition of electrolyte	0.05 M $CuSO_4$
ν (m^2/s)	1.0×10^{-6}
D_A (m^2/s)	6.5×10^{-10}
α_A (m^3/mol)	1.6×10^{-4}
${}^*t_1$	0.36
ρ_0 (kg/m^3)	0.99×10^3
σ (S/m)	0.5
Composition of electrolyte	0.05 M $CuSO_4$–1.85 M H_2SO_4
ν (m^2/s)	1.15×10^{-6}
D_A (m^2/s)	5.74×10^{-10}
α_A (m^3/mol)	1.25×10^{-4}
α_B (m^3/mol)	2.68×10^{-5}
${}^*t_1$	0.0033
${}^*t_2$	0.81
ρ_0 (kg/m^3)	1.12×10^3
σ (S/m)	51
a	0.31

2. The concentration fields of both Cu^{2+} and H^+ ions are numerically calculated according to Eq. 1, by solving Eq. 3 and 4 with boundary conditions based on the iterative algorithm.

3. Both anodic and cathodic current-density distributions along the vertical height are then calculated by correcting the electric-potential gradient toward the electrode surface to satisfy the constraint that the integration of local current density over the whole effective electrode surface area must be equal to the applied average current density i_{ave}. In this process, the iterative method is employed. The iteration is finished when the average current density estimated from the modified electric-potential gradient is converged within the error of 0.01% of the exact value.

4. Both velocity and pressure fields are calculated by numerically solving Eq. 6 and 7 with boundary conditions, according to the MAC method, where the iterative calculation method is used.

The convergence of the present calculation was examined with various kinds of time increment and spatial grid dimensions. There is almost no difference in the accuracy between the computational grids of 120×120 and 120×160 cells. In this study, the grid of 120×160 cells is adopted to examine the current-density distribution along the electrode height at an acceptable computing time. The time step Δt is set to 100 μs in the present calculation. The criteria of both $CuSO_4$ and H_2SO_4 concentration calculations at each time step are set to $2i_{ave}(1.0 - {}^*t_1)\sqrt{\Delta t}/z_1F\sqrt{\pi D_A}$ and $2i_{ave}({}^*t_2)\sqrt{\Delta t}/z_2F \times 1/\sqrt{\pi D_B}$, respectively, which are the measures of concentration change due to both diffusion and ionic migration effects at the initial time step. Besides, 0.1 μm/s is employed as the criterion of velocity calculation. The criterion of electric-potential calculation is 1 mV for the copper electrolysis in a 0.05 M $CuSO_4$ below $i = 1$ mA/cm^2 and in a 0.05 M $CuSO_4$–1.85 M H_2SO_4 below $i = 2$ mA/cm^2. For the copper electrolysis in a 0.05 M $CuSO_4$ above $i = 1$ mA/cm^2, 10 mV is adopted as the criterion. The physical properties employed in the present study are listed in Table II, which are referred to the previous studies.[9,10]

Results and Discussion

Figures 3 and 4 show the stream function profiles at 600 s after starting the galvanostatic electrolysis at various applied current densities in both electrolyte compositions. The cathode is placed on the left side and the anode on the right side. The similar stream function profiles and their transient phenomena have already been discussed previously.[13] The periodic fluctuating electrolyte flow phenomena are more remarkable in a 0.05 M $CuSO_4$ electrolyte solution, as seen in Fig. 3. At the higher current density, small vortices developing near both upper and lower edges of the effective electrodes significantly distort the flow pattern in the bulk electrolyte sandwiched by two vertical-plane electrodes. The periodically fluctuating electrolyte flow pattern then appears. Vortices' size seems to increase at the higher current density. The confinement effects, such as the collision between both cathodic upward and anodic downward natural convections and the effect caused by the insulated lateral wall and electrolyte free surfaces, may influence both concentration and current-density distributions along the electrode height. The confinement effects are less significant in a $CuSO_4$–H_2SO_4 electrolyte, as seen in Fig. 4. The addition of H_2SO_4 damps natural convection and prevents the further development to the transition or turbulent natural convection.

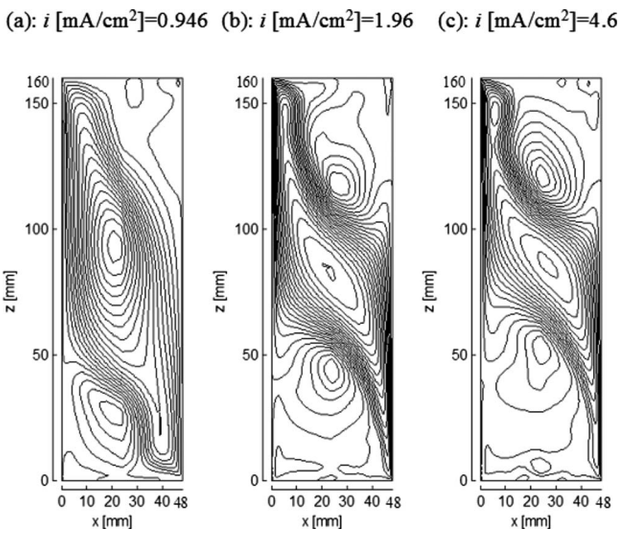

Figure 3. Stream function profile at 600 s after starting the electrolysis (0.05 M $CuSO_4$ solution, $t = 600$ s). (a) $i = 0.946$, (b) $i = 1.96$, and (c) $i = 4.6$ mA/cm^2.

The transient variations in the calculated electric-potential field are also shown in Fig. 5, where the galvanostatic copper electrolysis was carried out at $i = 0.946$ mA/cm^2 in a 0.05 M $CuSO_4$ aqueous electrolyte. The transient variations in the calculated electric-potential profile at the middle of the effective electrode height are also described in Fig. 6. The initially symmetric potential field is

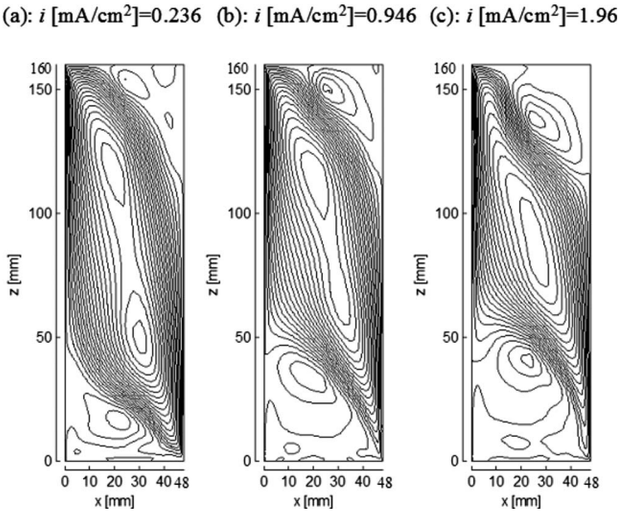

Figure 4. Stream function profile at 600 s after starting the electrolysis (0.05 M $CuSO_4$–1.85 M H_2SO_4 solution, $t = 600$ s). (a) $i = 0.236$, (b) $i = 0.946$, and (c) $i = 1.96$ mA/cm^2.

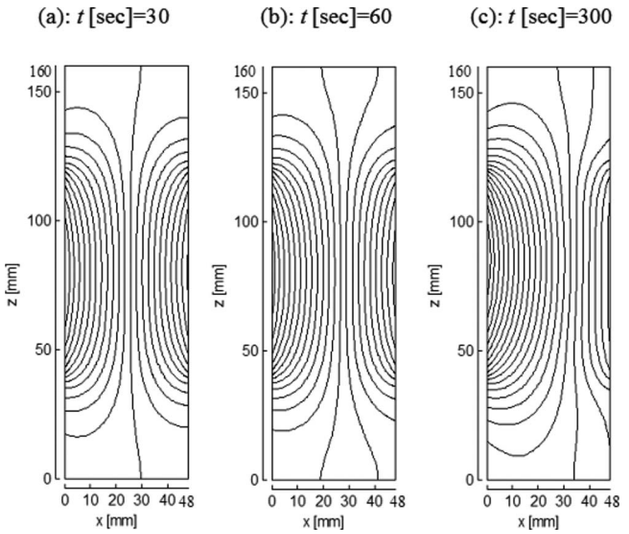

Figure 5. Transient variations in electric-potential field (0.05 M $CuSO_4$ solution, $i = 0.946$ mA/cm^2). (a) $t = 30$, (b) $t = 60$, and (c) $t = 300$ s.

gradually distorted with time. It is because the electric-potential gradient toward the cathode surface is steeper due to the depletion of the Cu^{2+}-ion concentration, while the electric-potential gradient toward the anode surface becomes more relaxed due to the enrichment of the Cu^{2+}-ion concentration. As the time progresses, the potential field starts to distort even along the vertical direction because both anode and cathode surface Cu^{2+}-ion concentrations vary with electrode height due to the development of natural convection.

The accuracy of present numerical calculation.— Figure 7 compares the transient variations in the calculated cathode surface Cu^{2+}-ion concentration with the analytical solutions at various current densities in a 0.05 M $CuSO_4$ aqueous electrolyte to check the accuracy of the present numerical calculation. The solid lines correspond to the analytical solutions, and the symbols correspond to the calculated results. Calculated results are plotted at 1 s intervals. The analytical solution for the transient variation in the electrode surface concentration is based on the unsteady one-dimensional diffusion equation in semi-infinite media, which can be expressed as follows

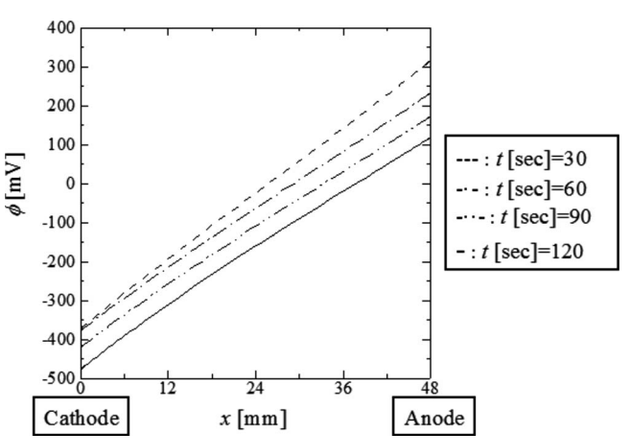

Figure 6. Transient variations in the electric-potential profile at midheight (0.05 M $CuSO_4$ solution, $i = 0.946$ mA/cm^2, $^*z = 4$ cm).

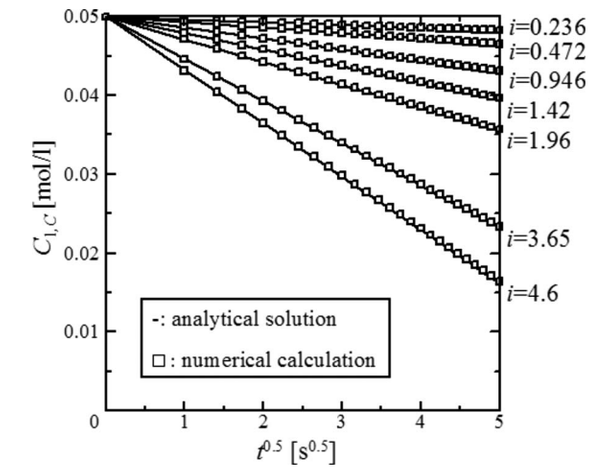

Figure 7. Transient variations in the cathode surface Cu^{2+}-ion concentration at midheight (0.05 M $CuSO_4$ solution, $^*z = 4$ cm).

$$C_{1,C}(t) = C_{1,0} + \frac{2(1.0 - {}^*t_1)i_{\text{ave}}}{z_1 F}\sqrt{\frac{t}{\pi D_A}} \qquad [47]$$

Because an electrolyte solution is initially homogeneous and at rest, the ionic mass-transfer phenomena due to both diffusion and ionic migration effects are predominant until natural convection starts to develop. The slopes estimated from the present calculation agree well with the analytical ones and the errors are within 1%.

Transient variations in ionic mass-transfer rate with natural convection.— Figure 8 compares the transient variations in the calcu-

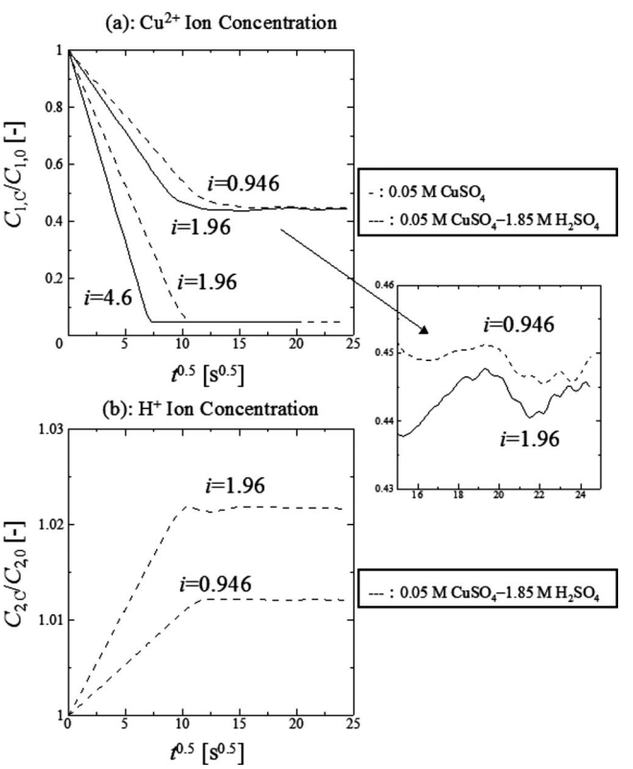

Figure 8. Transient variations in the calculated cathode surface ion concentration at midheight ($^*z = 4$ cm). (a) Cu^{2+}-ion concentration and (b) H^+-ion concentration.

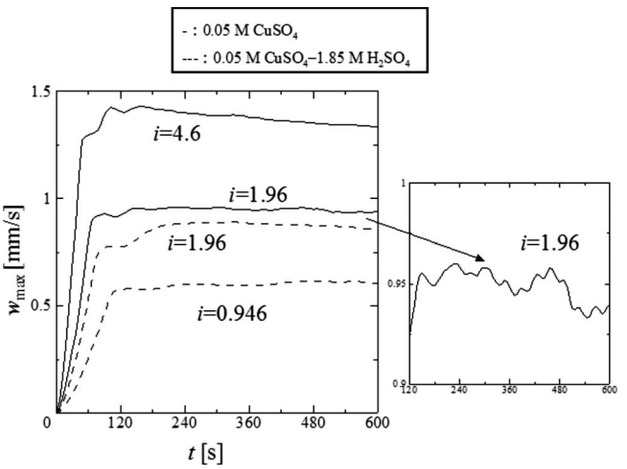

Figure 9. Transient variations in maximal natural convective velocity at midheight ($^{*}z = 4$ cm).

lated cathode surface ion concentration at the middle of the height between a $CuSO_4$ aqueous electrolyte with and without H_2SO_4. The solid lines correspond to the calculated results in a 0.05 M $CuSO_4$, while the dashed lines to those in a 0.05 M $CuSO_4$–1.85 M H_2SO_4. Calculated results are plotted at 6 s intervals. Clearly the Cu^{2+}-ion concentration decreases due to the electrodeposition of copper at the cathode surface, while the H^+-ion concentration increases due to the ionic migration effect. These concentration changes are initially proportional to the square root of duration time, which implies that the ionic mass-transfer phenomena due to both diffusion and ionic migration effects are dominant just after stating the electrolysis.

As time progresses, natural convection develops along the vertical-plane cathode. The cathode surface ion concentration gradually approaches a substantially steady-state value. It is almost similar to the previous study[12] where the galvanostatic copper electrolysis was carried out in a smaller electrolytic cell with a height of 10 mm and an electrode spacing of 1–2 mm. The most different point from the previous study is that it takes more time to attain a substantial steady state in the present study. It is ascribed to the cell dimensions such as the interelectrode distance and electrode height, which are deeply related to the magnitude of the developed natural convection, the collision and interaction between anodic downward and cathodic upward natural convections. The electrode surface concentration gradually converges to an almost steady-state value with fluctuation, and its amplitude of oscillation becomes larger at the higher current density in an unsupported $CuSO_4$. The interaction behavior between cathodic upward and anodic downward natural convections induces such a fluctuation. The periodic fluctuating electrolyte flow phenomena resulting from such an interaction lasts a much longer time because they are related to the momentum dissipation by viscous stress.

The similar fluctuating behaviors are also seen in Fig. 9, which describes the transient variations in the maximal natural convective velocity w_{max} at the middle of the height in two different electrolyte solutions at various current densities. The solid lines correspond to the calculated results in a 0.05 M $CuSO_4$, while the dashed lines to those in a 0.05 M $CuSO_4$–1.85 M H_2SO_4. Calculated results are plotted at 6 s intervals. The maximum value of the natural convective velocity in the hydrodynamic boundary layer is located at 300–600 μm away from the electrode surface. Because the buoyancy of H_2SO_4 induced by the ionic migration effect acts in an opposite direction to that of $CuSO_4$, the magnitude of the developed natural convection is depressed in a 0.05 M $CuSO_4$–1.85 M H_2SO_4. The overshoots followed by fluctuating phenomena are clearly seen in both electrolyte solutions. The similar results were also seen in the previous study in a tiny electrolytic cell.[12] Compared to the previous study, the following two things are noted.

1. The magnitude of the overshoot is smaller in the present electrolytic cell.
2. It takes much more time to approach a substantial steady-state value in the present study than in the previous study.

As already mentioned in oscillation behaviors of the concentration, the overshoot followed by fluctuating behaviors in velocity is also determined by the magnitude of the applied current density, cell dimensions, and electrode configuration.

The interesting result is that the calculated maximal velocity starts to decrease almost monotonously at 240 s after stating the electrolysis at $i = 4.6$ mA/cm^2 in a 0.05 M $CuSO_4$ aqueous electrolyte. Such a phenomenon could not be detected in previous studies.[12,13] This apparent deceleration in the natural convective velocity is ascribed to the electrolyte stratification near the upper cathode, where the lighter and lower concentration electrolyte is accumulated. It is considered as very important in the electrolyte circulation system design in the actual industrial electrorefining tankhouse because the conventional electrorefining operation lasts for several weeks.

The transient variations in the maximal natural convective velocity take much more time to approach a substantial steady state compared to the transient variations in the electrode surface concentration. Because the CBL thickness is very thin compared to the hydrodynamic boundary-layer thickness because of the high Schmidt number, the effect of secondary flow velocity changes on the convective mass transfer is far less significant. Therefore, the concentration fluctuation in the CBL is damped out more rapidly than the velocity fluctuation in the hydrodynamic boundary layer.

Current-density distribution along the vertical cathode.— Figure 10 shows the calculated cathodic current-density distribution along the vertical height at 600 s after starting the electrolysis in both electrolyte compositions at various current densities. Here, $^{*}z$ is the vertical distance from the lower edge of the effective cathode. The present calculation predicts that the uniform current-density distribution is maintained within 600 s except for $i = 3.65$ and 4.6 mA/cm^2 in a 0.05 M $CuSO_4$ and $i = 1.96$ mA/cm^2 in a 0.05 M $CuSO_4$–1.85 M H_2SO_4. At $i = 3.65$ mA/cm^2 in a 0.05 M $CuSO_4$, the partial limiting current condition is established, while the entire limiting current conditions are established at $i = 4.6$ mA/cm^2 in a 0.05 M $CuSO_4$ and at $i = 1.96$ mA/cm^2 in a 0.05 M $CuSO_4$–1.85 M H_2SO_4.

Typical transient variations in the cathodic current density and corresponding cathode surface Cu^{2+}-ion concentration distributions along the vertical height are also seen in Fig. 11. The cathode surface Cu^{2+}-ion concentration decreases with height as the natural convection develops along the vertical cathode with time. Thus, the partial limiting current condition is established at the upper cathode when a high level constant current is imposed. A relatively localized peak appears due to mass-transfer limitation at the upper cathode, and this peak descends from the upper end to the lower end with time.

As long as the cathode surface is flat and natural convection is steady laminar flow in semi-infinite media, the boundary-layer theory gives the following expression under the presumption of uniform distribution of the zero concentration of the Cu^{2+} ion along the cathode height (detail derivation has been described in Ref. 1 and 3)

$$i_C(^{*}z) \propto {}^{*}z^{-0.25} \qquad [48]$$

Figure 12 demonstrates the relationships between $\log(^{*}z/h)$ and $\log[i_C(^{*}z)/i_{ave}]$ at 600 s after starting the electrolysis in both electrolyte compositions at the experimentally measured limiting current densities. Here, h is the height of the effective electrode. The boundary-layer theory qualitatively agrees with the calculated slope in both electrolyte solutions. The small differences are attributed to

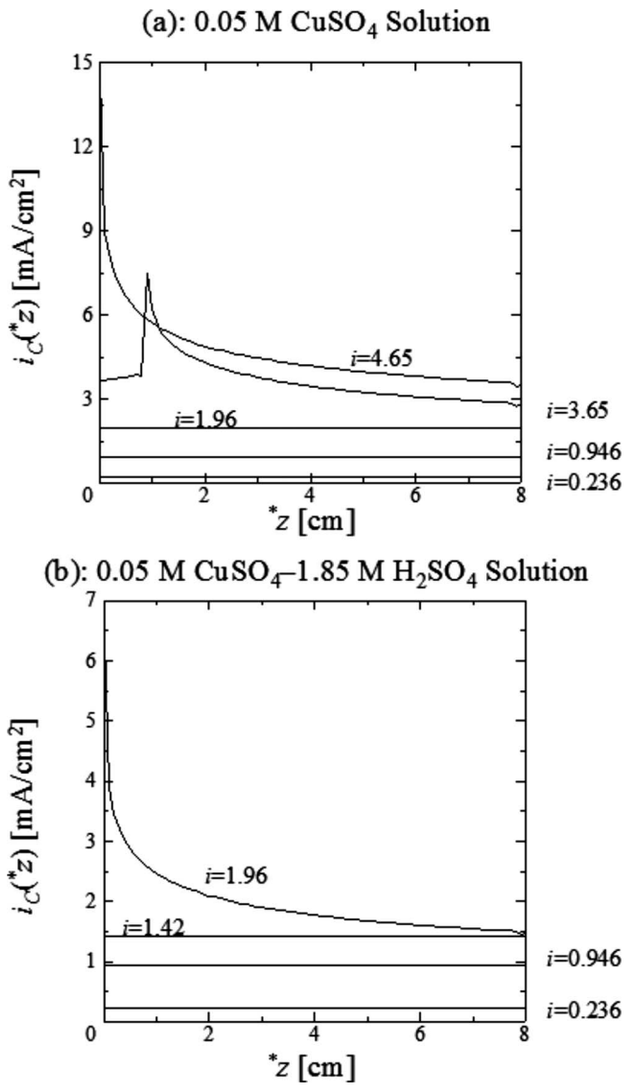

Figure 10. Calculated current-density distribution along the vertical cathode height at 600 s after starting the electrolysis at various current densities (t = 600 s). (a) 0.05 M $CuSO_4$ solution and (b) 0.05 M $CuSO_4$–1.85 M H_2SO_4 solution.

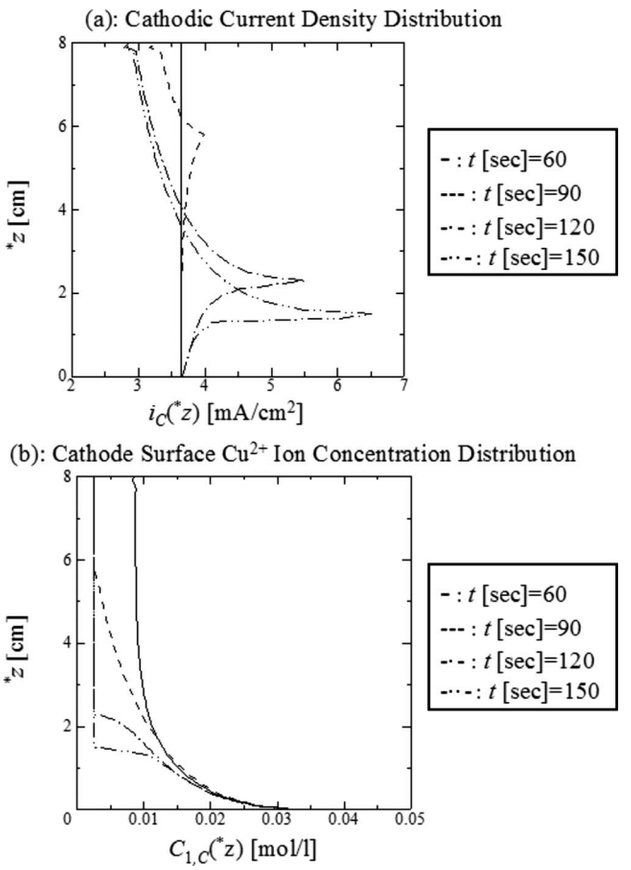

Figure 11. Transient variations in the calculated cathodic current density and Cu^{2+}-ion concentration distributions along the vertical height (0.05 M $CuSO_4$ solution, i = 3.65 mA/cm^2). (a) Cathodic current-density distribution and (b) cathode surface Cu^{2+}-ion concentration distribution.

finite electrode height and interelectrode distance as well as the breakdown of the steady laminar electrolyte flow, as seen in Fig. 3 and 4.

Correction factor ε.— The difficulty to numerically predict the limiting current density in an unsupported $CuSO_4$ electrolyte solution accompanies how to express the ionic migration effect in the zero concentration electrolyte solution. Because the conventional transference number treatment no longer becomes available, it is hard to accurately estimate the contribution of ionic migration effect to the ionic mass flux.

Figure 13 shows the transient variations in calculated correction factor ε in both electrolyte solutions at the experimentally measured limiting current densities. Before establishing the entire limiting current condition, ε is maintained at constant values of 1.56 in the $CuSO_4$ electrolyte and 1.003 in the $CuSO_4$–H_2SO_4 electrolyte, respectively. It is because ε is expressed in terms of the transference number of the Cu^{2+} ion as follows

$$\varepsilon = \frac{I_L}{I_D} = \frac{1.0}{1.0 - {}^{*}t_1} \qquad [49]$$

After establishing the entire limiting current condition, ε starts to increase. At the experimentally measured limiting current density, ε approaches 1.7 in the $CuSO_4$ electrolyte and 1.03 in the $CuSO_4$–H_2SO_4 electrolyte, respectively. The calculated value of ε gradually decreases with oscillation at i = 4.6 mA/cm^2 in the $CuSO_4$ electrolyte. There exists no numerical study on the transient variations in the correction factor ε in the electrolytic process with vertical-plane electrode configuration. Newman examined the dependence of ε on the additive amount of H_2SO_4 with the rotating-disk electrode in a $CuSO_4$–H_2SO_4 aqueous electrolyte solution, [29] where ε was estimated around 1.9 in an unsupported $CuSO_4$. This value agrees well with the present numerical calculation, as far as the transient variation in ε is concerned. However, further numerical study is indispensable to examine the validity of the present numerical estimation of ionic migration effect under the limiting current condition because only two cases are numerically calculated in this study.

Conclusion

The mathematical model for the ionic mass-transfer rates associated with natural convection induced along the vertical-plane electrodes in an aqueous electrolyte solution is developed. The effects of a supporting electrolyte and an interaction between both cathodic and anodic natural convections on the ionic mass-transfer rate are examined.

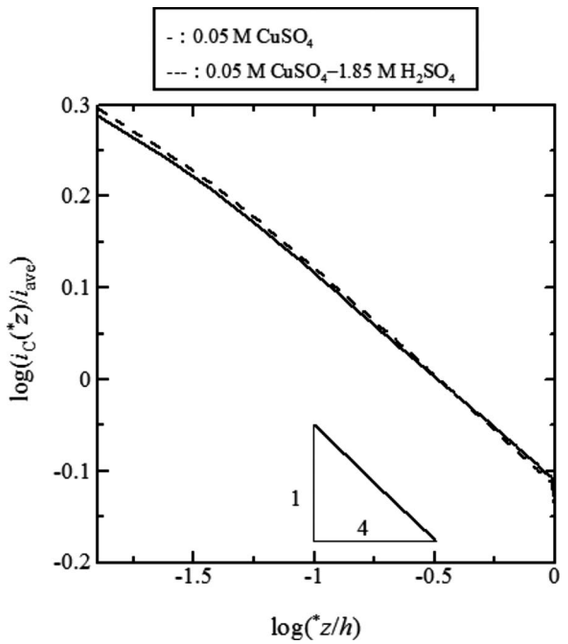

Figure 12. Relationships between $\log({}^{*}z/h)$ and $\log(i_C/i_{ave})$ at (t = 600 s). -: 0.05 M $CuSO_4$ solution, i = 4.6 mA/cm^2. ---: 0.05 M $CuSO_4$–1.85 M H_2SO_4 solution, i = 1.96 mA/cm^2.

The present calculation predicts that the uniform current-density distribution can be maintained within 600 s after starting the galvanostatic electrolysis below one-half of the limiting current density in both electrolyte compositions. Both partial and entire limiting current conditions along the vertical cathode are calculated. Under the entire limiting current condition, the classical natural convection correlation for the vertical cathode qualitatively agrees with the present numerical calculation. The deceleration in the natural convective velocity is noticed at the high level constant current density in a 0.05 M $CuSO_4$, which is ascribed to the electrolyte stratification.

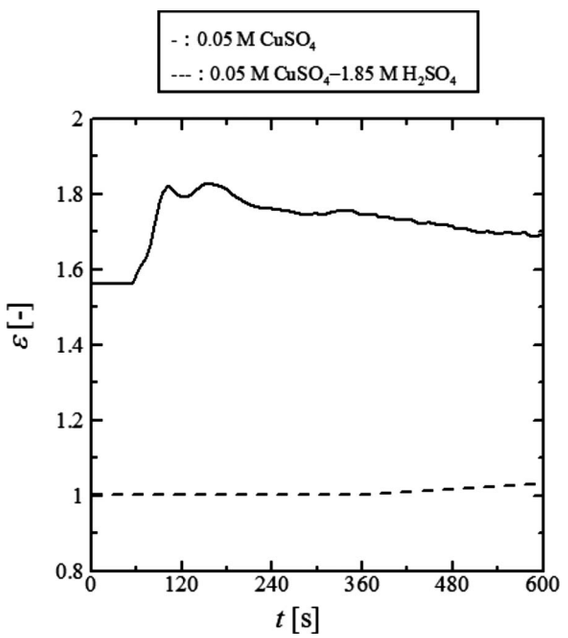

Figure 13. Transient variations in the calculated correction factor ε in two electrolyte solutions. -: 0.05 M $CuSO_4$ solution, i = 4.6 mA/cm^2. ---: 0.05 M $CuSO_4$–1.85 M H_2SO_4 solution, i = 1.96 mA/cm^2.

List of Symbols

a	degree of dissociation of the HSO_4^- ion
A	total effective electrode surface area, m^2
C_i	concentration of an ion species i, mol m^{-3}
$C_{i,0}$	concentration of an ion species i in the bulk electrolyte, mol m^{-3}
$C_{i,C}$	concentration of an ion species i at the cathode surface, mol m^{-3}
D_i	diffusion coefficient of an ion species or electroneutral compound i, m^2 s^{-1}
F	Faraday constant, 96,500 C/equiv
g	gravitational acceleration, 9.8 m s^{-2}
$\mathbf{g}$	gravitational acceleration vector, m s^{-2}
h	height of the effective electrode, m
H	height of an electrolyte free surface from the bottom of a cell, m
i	current density, A m^{-2}
i_{ave}	average current density, A m^{-2}
i_A	anodic current density, A m^{-2}
i_C	cathodic current density, A m^{-2}
$i_{D,C}$	cathodic diffusion current density, A m^{-2}
I_D	limiting diffusion current over the whole effective electrode area, A
I_L	limiting current over the whole effective electrode area, A
j_k	mass flux of ion species k, mol m^{-2} s^{-1}
L	interelectrode spacing, m
m_i	concentration of an electroneutral compound i, mol m^{-3}
$m_{i,0}$	concentration of an electroneutral compound i in the bulk electrolyte, mol m^{-3}
n	normal direction to the boundary
P	pressure, N m^{-2}
R	universal gas constant, 8.314 J mol^{-1} K^{-1}
t	time, s
${}^{*}t_i$	transference number of an ion species i
T	temperature, K
u	horizontal component of fluid velocity of an electrolyte, m s^{-1}
$\mathbf{v}$	fluid velocity vector, m s^{-1}
w	vertical component of fluid velocity of an electrolyte, m s^{-1}
w_{max}	maximum value of natural convective velocity, m s^{-1}
x	horizontal distance from the cathode surface, m
${}^{*}x$	horizontal distance from the anode surface, m
z	vertical distance from the bottom of a cell, m
z_i	valency of an ion species i, g equiv mol^{-1}
${}^{*}z$	vertical distance from the lower edge of the effective electrode, m

Greek

α_i	densification coefficient of an electroneutral compound i, m^3 mol^{-1}
Δm_i	concentration difference in an electroneutral compound i from the bulk electrolyte, mol m^{-3}
$\Delta\rho$	fluid density difference from bulk electrolyte, kg m^{-3}
ε	correction factor
ζ	ratio of concentration gradient of the SO_4^{2-} ion to the Cu^{2+} ion at the electrode surface
η	ratio of concentration gradient of the HSO_4^- ion to the Cu^{2+} ion at the electrode surface
μ_i	mobility of an ion species i, m^2 V^{-1} s^{-1}
ν	kinematic viscosity of an electrolyte, m^2 s^{-1}
ξ	ratio of concentration gradient of the H^+ ion to the Cu^{2+} ion at the electrode surface
ρ	fluid density of an electrolyte, kg m^{-3}
ρ_0	fluid density of bulk electrolyte, kg m^{-3}
σ	electric conductivity of an electrolyte, S m^{-1}
ϕ	electric potential, V

Subscripts

0	reference value
1	Cu^{2+} ion
2	H^+ ion
3	HSO_4^- ion
4	SO_4^{2-} ion
A	$CuSO_4$
B	H_2SO_4
LS	at the electrolyte free surface
S	at the electrode or lateral wall surfaces
WS	at the bottom wall surface

Waseda University assisted in meeting the publication costs of this article.

References

1. C. Wagner, *J. Electrochem. Soc.*, **95**, 161 (1949).
2. N. Ibl and R. H. Muller, *J. Electrochem. Soc.*, **105**, 346 (1958).
3. C. R. Wilke, M. Eisenberg, and C. W. Tobias, *J. Electrochem. Soc.*, **100**, 513 (1953).
4. C. Wagner, *J. Electrochem. Soc.*, **98**, 116 (1951).
5. A. Brenner, *Tech. Proc. Am. Electroplat. Soc.*, **27**, 95 (1940).
6. K. Asada, F. Hine, S. Yoshizawa, and S. Okada, *J. Electrochem. Soc.*, **107**, 242 (1960).
7. Y. Konishi, Y. Tanaka, Y. Kondo, and Y. Fukunaka, *Electrochim. Acta*, **46**, 681 (2000).
8. Y. Awakura, A. Ebata, and Y. Kondo, *J. Electrochem. Soc.*, **126**, 23 (1979).
9. Y. Fukunaka, K. Denpo, M. Iwata, K. Maruoka, and Y. Kondo, *J. Electrochem. Soc.*, **130**, 2492 (1983).
10. Y. Fukunaka, Y. Nakamura, and Y. Konishi, *J. Electrochem. Soc.*, **145**, 3814 (1998).
11. K. Denpo, T. Okumura, Y. Fukunaka, and Y. Kondo, *J. Electrochem. Soc.*, **132**, 1145 (1985).
12. S. Kawai, K. Nishikawa, Y. Fukunaka, and S. Kida, *Electrochim. Acta*, **53**, 257 (2007).
13. S. Kawai, Y. Fukunaka, and S. Kida, *J. Electrochem. Soc.*, **155**, F75 (2008).
14. J. Newman, *J. Electrochem. Soc.*, **113**, 1235 (1966).
15. V. Marathe and J. Newman, *J. Electrochem. Soc.*, **116**, 1704 (1969).
16. W. H. Smyrl and J. Newman, *J. Electrochem. Soc.*, **118**, 1079 (1971).
17. R. V. Homsy and J. Newman, *J. Electrochem. Soc.*, **121**, 521 (1974).
18. C. M. Mohr, Jr. and J. Newman, *J. Electrochem. Soc.*, **123**, 1687 (1976).
19. W. R. Parrish and J. Newman, *J. Electrochem. Soc.*, **116**, 169 (1969).
20. W. R. Parrish and J. Newman, *J. Electrochem. Soc.*, **117**, 43 (1970).
21. R. Alkire and A. A. Mirarefi, *J. Electrochem. Soc.*, **120**, 1507 (1973).
22. R. Alkire and A. A. Mirarefi, *J. Electrochem. Soc.*, **124**, 1043 (1977).
23. R. Alkire and A. A. Mirarefi, *J. Electrochem. Soc.*, **124**, 1214 (1977).
24. M. Georgiadou, *J. Electrochem. Soc.*, **144**, 2732 (1997).
25. F. H. Bark and F. Alavyoon, *J. Fluid Mech.*, **290**, 1 (1995).
26. V. M. Volgin, O. V. Volgina, D. A. Bograchev, and A. D. Davydov, *J. Electroanal. Chem.*, **546**, 15 (2003).
27. Y. Fukunaka, H. Doi, and Y. Kondo, *J. Electrochem. Soc.*, **137**, 88 (1990).
28. J. R. Selman and J. Newman, *J. Electrochem. Soc.*, **118**, 1070 (1971).
29. J. Newman, *Electrochemical Systems*, Prentice-Hall, Englewood Cliffs, NJ (1973).
30. A. Eklund, F. Alavyoon, D. Simonsson, R. I. Karlsson, and F. H. Bark, *Electrochim. Acta*, **36**, 1345 (1991).